JOURNAL OF COMPUTATIONAL PHYSICS **125,** 440–453 (1996)
ARTICLE NO. 0106

2D Orthogonal Grid Generation with Boundary Point Distribution Control

LUIS EÇA

MARETEC, Mechanical Engineering Department, Instituto Superior Técnico, Technical University of Lisbon, Lisbon, Portugal

Received May 3, 1995; revised October 23, 1995

A numerical method for 2D orthogonal grid generation with control of the boundary point distribution is presented. The method is based on the solution of a system of partial differential equations. The grid cell aspect ratio, the so-called distortion function, is calculated from its definition equation in the entire domain. The method allows the specification of the boundary point distribution in all the boundaries and also the distance of the first grid node to the boundary. The method is successfully applied to several geometries, including geometries with grid singularities and grids around airfoils and cross-sections of ship sterns.

1. INTRODUCTION

A successful numerical calculation of a set of partial differential equations is strongly dependent on a good ''quality'' grid. Among the several aspects that may characterize the grid ''quality,'' its orthogonality is usually considered one of the most important. Two-dimensional orthogonal grid generators have been the subject of many works published in the literature since the early 1980s, like for example, [1–13].

A classical approach to this problem is the use of conformal mapping. An example of its application is given by Moretti in [11]. However, conformal mapping is not very flexible in the control of the grid node distribution, which penalizes its application to difficult geometries [13].

One of the most popular ways of generating orthogonal grids is to use a set of partial differential equations. Different generating systems have been proposed since the work of Mobley and Stewart in 1980 [1]. Visbal and Knight in 1982 [3] applied the widely used elliptic system proposed by Thompson *et al.* [14] with the ''control functions'' determined in such a way that the generated grid would be either orthogonal or nearly orthogonal. A similar elliptical system has been used by Steger and Sorenson in the GRAPE code [15], where the ''control functions'' are calculated iteratively to obtain grid orthogonality and a specified grid spacing at the boundary. However, the interior grid lines may exhibit large deviations from orthogonality. A different elliptic system was proposed by Thompson *et al.* in [16]. This generating system was adopted by Ryskin and Leal in [4].

Ryskin and Leal classified their method in two categories: the ''weak constraint'' and ''strong constraint'' methods, according to the type of boundary conditions adopted [4]. The ''strong constraint'' method applies to domains whose shape is not known in advance and the ''weak constraint'' method, to domains with a known shape. The latter one has been the subject of several papers [5, 7, 12, 13] which investigated the conditions under which the generating system of equations would generate orthogonal grids. The main topic of discussion is the existence of a unique solution for the set of partial differential equations adopted by Ryskin and Leal [4] and the type of boundary conditions that would be admissible to obtain orthogonal grids. Namely, the number of boundaries where the boundary point distribution may be prescribed.

Most of the theoretical work published in these papers is based on quasi-conformal mapping [17]. In many of these approaches the grid cell aspect ratio, which is defined by the so-called distortion function, is specified by an auxiliary equation or by interpolation from the boundaries, which limits the number of boundaries where the grid nodes may be specified [6]. It is commonly accepted that the ''weak constraint'' method of Ryskin and Leal [4], where the boundary point distribution is specified in all the boundaries and the distortion function is interpolated from the boundary values, in general, produces only nearly orthogonal grids [5].

The present paper addresses the problem of 2D orthogonal grid generation with specified boundary point distribution in all the boundaries in a purely numerical way. The present technique has been suggested by Albert in [8], but not convincingly explored. In a recent paper Allievi and Calisal [12] also use a similar technique. However, Allievi and Calisal concluded that their method is successful due to a Bubnov–Galerkin formulation, rather than the way in which the distortion function is calculated. In the present technique the distortion function is calculated from its definition equation in all the domain. Our aim is to demonstrate that it is possible to obtain orthogonal grids with

0021-9991/96 $18.00

this type of boundary condition for a large variety of geometries. In addition, we show that the distance of the first grid node to the boundary may also be specified, which may be an advantageous feature for near-wall viscous flows. Boundary conditions which allow the grid nodes to move along the lines that define the boundary are also explored.

2. GENERATING SYSTEM

A 2D orthogonal grid satisfies the condition

$$g_{12} = \frac{\partial x}{\partial \xi}\frac{\partial x}{\partial \eta} + \frac{\partial y}{\partial \xi}\frac{\partial y}{\partial \eta} = 0, \tag{1}$$

where g_{12} is the off-diagonal component of the covariant metric tensor. From Eq. (1) and the condition that the Jacobian of the transformation should be greater than zero it is easy to see that a 2D orthogonal grid also satisfies the Beltrami equations [16], which may be viewed as generalizations of the Cauchy–Riemann equations [13].

$$\begin{aligned} \frac{\partial x}{\partial \eta} &= -f\frac{\partial y}{\partial \xi}, \\ \frac{\partial y}{\partial \eta} &= f\frac{\partial x}{\partial \xi}, \end{aligned} \tag{2}$$

where the so-called distortion function, f, is a positive quantity given by the ratio of the scale factors h_η and h_ξ,

$$f = \frac{h_\eta}{h_\xi} \tag{3}$$

and

$$\begin{aligned} h_\eta &= \sqrt{g_{22}} = \sqrt{(\partial x/\partial \eta)^2 + (\partial y/\partial \eta)^2}, \\ h_\xi &= \sqrt{g_{11}} = \sqrt{(\partial x/\partial \xi)^2 + (\partial y/\partial \xi)^2}. \end{aligned} \tag{4}$$

From the Beltrami equations, (2), and the equalities

$$\begin{aligned} \frac{\partial}{\partial \eta}\left(\frac{\partial x}{\partial \xi}\right) &= \frac{\partial}{\partial \xi}\left(\frac{\partial x}{\partial \eta}\right), \\ \frac{\partial}{\partial \eta}\left(\frac{\partial y}{\partial \xi}\right) &= \frac{\partial}{\partial \xi}\left(\frac{\partial y}{\partial \eta}\right), \end{aligned}$$

the set of partial differential equations used by Ryskin and Leal, [4], is easily derived:

$$\begin{aligned} \frac{\partial}{\partial \xi}\left(f\frac{\partial x}{\partial \xi}\right) + \frac{\partial}{\partial \eta}\left(\frac{1}{f}\frac{\partial x}{\partial \eta}\right) &= 0, \\ \frac{\partial}{\partial \xi}\left(f\frac{\partial y}{\partial \xi}\right) + \frac{\partial}{\partial \eta}\left(\frac{1}{f}\frac{\partial y}{\partial \eta}\right) &= 0. \end{aligned} \tag{5}$$

This generating system has been used by several authors, for example [5, 6, 8, 12, 13]. The differences between the methods proposed by these authors is the way in which the distortion function f is obtained. Three types of procedures have been proposed:

1. Calculate f from its definition equation, (3), at the boundaries and obtain the values in the domain by interpolation or solving a Laplace equation [4].

2. Specify a class of admissible functions for f which guarantees the existence of a unique solution [6, 13].

3. Calculate f from its definition equation, (3), in the entire domain [8, 12].

The way in which f is obtained clearly affects the type of boundary conditions that can be applied to obtain orthogonal grids. The first option corresponds to the "weak constraint" method of Ryskin and Leal, where the boundary point distribution is specified in all the boundaries. However, the application of this technique to different geometries has shown that the method produces only nearly orthogonal grids [5]. In the second option, the calculation of f is usually based on the theory of quasi-conformal mapping and the number of boundaries where the boundary point distribution can be specified varies from zero [13] to two [6]. The latter option has been used by Albert [8] and Allievi and Calisal [12] with the boundary-point distribution specified in all the boundaries, using two different numerical approaches. The examples presented in these papers are similar. Although the number of grid nodes used by Albert in [8] is rather small, the results of the two numerical solutions indicate that the success of the approach must be due to the way in which the distortion function is calculated, rather than to the Bubnov–Galerkin formulation as claimed by Allievi and Calisal [12]. Therefore, to be able to specify the boundary point distribution in all the boundaries we calculate the distortion function from its definition equation (3), in all the domain.

The system of partial differential equations (5), with f calculated from its definition equation (3), is a nonlinear system which implies that the solution must be obtained by an iterative procedure. The following iterative algorithm is used to solve the nonlinear system of partial differential equations (5):

1. Determine an initial approximation for the grid. In the present method, we use linear transfinite interpolation.

2. Calculate the distortion function from the available grid using Eq. (3).

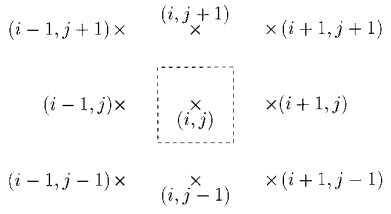

FIG. 1. Typical control "volume" used in the discretization.

3. Solve the system of Eqs. (5) with f fixed.

4. Go back to step 2 if the convergence criteria are not satisfied.

The convergence criteria are discussed in Section 3.5.

2.1. *Boundary Conditions*

The system of partial differential equations (5) requires boundary conditions at the four boundaries of the computational domain. Two types of boundary conditions are available:

• Dirichlet boundary conditions. The coordinates (x, y) of the grid nodes are specified.

• Neumann–Dirichlet boundary conditions. The grid nodes satisfy the orthogonality condition, Eq. (1) [Neumann], and the equation that defines the boundary line [Dirichlet].

The present choice is to use Dirichlet boundary conditions in all the boundaries. Although we do not have any theoretical proof that the system of partial differential equations (5), with f obtained from its definition equation (3), with this type of boundary conditions, has a unique solution, or even any solution, we will show numerically that it is possible to obtain converged solutions. Furthermore, we will also show that it is also possible to specify the distance of the first grid node to the boundary, which may be a very attractive feature for viscous flows calculations in computational fluid dynamics.

The use of boundary conditions of the second type, Neumann–Dirichlet, which are mandatory in at least two boundaries for the approaches based in quasi-conformal mapping [6] is also explored. The application of this type of boundary conditions is investigated with and without specified distance of the first grid node to the boundary. The boundary line is defined by a cubic "spline" calculated with the initial boundary point distribution.

3. NUMERICAL SOLUTION

3.1. *Discretized Equations*

The present grid generating system, given by the system of partial differential equations (5), is discretized using a control "volume" technique. The unknowns are collocated at the center of the "volume" as shown in Fig. 1. Integrating both terms of Eqs. (5) in a typical control "volume," we obtain

$$\begin{aligned}
&f_{i+1/2,j}\left(\frac{\partial x}{\partial \xi}\right)_{i+1/2,j} - f_{i-1/2,j}\left(\frac{\partial x}{\partial \xi}\right)_{i-1/2,j} \\
&\quad + \frac{1}{f_{i,j+1/2}}\left(\frac{\partial x}{\partial \eta}\right)_{i,j+1/2} - \frac{1}{f_{i,j-1/2}}\left(\frac{\partial x}{\partial \eta}\right)_{i,j-1/2} = 0, \\
&f_{i+1/2,j}\left(\frac{\partial y}{\partial \xi}\right)_{i+1/2,j} - f_{i-1/2,j}\left(\frac{\partial y}{\partial \xi}\right)_{i-1/2,j} \\
&\quad + \frac{1}{f_{i,j+1/2}}\left(\frac{\partial y}{\partial \eta}\right)_{i,j+1/2} - \frac{1}{f_{i,j-1/2}}\left(\frac{\partial y}{\partial \eta}\right)_{i,j-1/2} = 0,
\end{aligned} \tag{6}$$

where the indexes (i, j) refer to the directions ξ and η, respectively.

Using second-order central differences for the first derivatives of the grid coordinates and, assuming that the grid line spacing in the computational domain is uniform and equal to one, the set of partial differential equations (5) is transformed into the system of algebraic equations,

$$\begin{aligned}
&f_{i+1/2,j}x_{i+1,j} + f_{i-1/2,j}x_{i-1,j} + \frac{1}{f_{i,j+1/2}}x_{i,j+1} \\
&\quad + \frac{1}{f_{i,j-1/2}}x_{i,j-1} - F_{i,j}x_{i,j} = 0, \\
&f_{i+1/2,j}y_{i+1,j} + f_{i-1/2,j}y_{i-1,j} + \frac{1}{f_{i,j+1/2}}y_{i,j+1} \\
&\quad + \frac{1}{f_{i,j-1/2}}y_{i,j-1} - F_{i,j}y_{i,j} = 0,
\end{aligned} \tag{7}$$

where

$$F_{i,j} = f_{i+1/2,j} + f_{i-1/2,j} + \frac{1}{f_{i,j+1/2}} + \frac{1}{f_{i,j-1/2}}.$$

3.2. *Solution Procedure*

Equations (7) represent a coupled, nonlinear, system of algebraic equations, due to the dependence of f on x and y. The linearization of the system of algebraic equations is performed calculating f from a previous approximation of the solution. For each step of this iterative process, Eqs. (7) become an uncoupled linear system of algebraic equations which has to be solved to obtain the new approximation of the solution. The iterative process required to determine f from its definition equation (3) will be referred to as the global cycle.

The linear system of algebraic equations is solved by successive line overrelaxation (SLOR), which is an iterative technique. The initial approximation to this iteration

cycle is the grid calculated with the values of f from the previous iteration. The overrelaxation parameter is estimated using the technique proposed by Ehrlich in [18]. The iterative cycle required by the SLOR will be referred to as the inner cycle.

3.3 *Determination of f*

The coefficients of the algebraic system of Eqs. (7) are the distortion function values at the four boundaries of the control "volume." To calculate f at these four boundaries, the first derivatives of the grid coordinates are approximated by first-order central differences. At each boundary, this is a straightforward procedure to obtain two of the four derivatives involved in the determination of f like, for example, the derivatives in the ξ direction for the boundaries at $(i - 1/2, j)$ and $(i + 1/2, j)$. However, the remaining two derivatives require values of the grid coordinates at the corners of the control "volume." Thompson in [19] suggests that an auxiliary grid, with the nodes located at the corners of the control "volume" illustrated in Fig. 1, can be used to obtain the unknown grid coordinates. The main drawback of this approach is the double effort required to generate the grid. In the present method we adopted a much simpler technique. The unknown grid coordinates are calculated from the arithmetic mean of the four surrounding nodes. Therefore, we obtain:

$$
\begin{aligned}
f_{i+1/2,j} &\simeq \frac{1}{2}\sqrt{\frac{(x_{i+1,j+1}+x_{i,j+1}-x_{i+1,j-1}-x_{i,j-1})^2+(y_{i+1,j+1}+y_{i,j+1}-y_{i+1,j-1}-y_{i,j-1})^2}{(x_{i+1,j}-x_{i,j})^2+(y_{i+1,j}-y_{i,j})^2}}\\
f_{i-1/2,j} &\simeq \frac{1}{2}\sqrt{\frac{(x_{i-1,j+1}+x_{i,j+1}-x_{i-1,j-1}-x_{i,j-1})^2+(y_{i-1,j+1}+y_{i,j+1}-y_{i+1,j-1}-y_{i,j-1})^2}{(x_{i,j}-x_{i-1,j})^2+(y_{i,j}-y_{i-1,j})^2}}\\
f_{i,j+1/2} &\simeq 2\sqrt{\frac{(x_{i,j+1}-x_{i,j})^2+(y_{i,j+1}-y_{i,j})^2}{(x_{i+1,j}+x_{i+1,j+1}-x_{i-1,j}-x_{i-1,j+1})^2+(y_{i+1,j}+y_{i+1,j+1}-y_{i-1,j}-y_{i-1,j+1})^2}}\\
f_{i,j-1/2} &\simeq 2\sqrt{\frac{(x_{i,j}-x_{i,j-1})^2+(y_{i,j}-y_{i,j-1})^2}{(x_{i+1,j}+x_{i+1,j-1}-x_{i-1,j}-x_{i-1,j+1})^2+(y_{i+1,j}+y_{i+1,j-1}-y_{i-1,j}-y_{i-1,j+1})^2}}
\end{aligned}
\tag{8}
$$

Equations (8) are applied to the grid coordinates of the available approximation of the solution. The maximum relative difference of f between iterations, ϕ_f, with

$$\phi_f = \max\left(\frac{f^n - f^{n-1}}{f^n}\right), \tag{9}$$

is used to monitor the convergence of the distortion function. The superscript ^{n} refers to the global iteration level.

3.4. *Boundary Conditions*

The application of Dirichlet boundary conditions is straightforward. If Neumann–Dirichlet boundary conditions are applied at a boundary, the condition $g_{12} = 0$, Eq. (1), must be satisfied and the grid node must also belong to the line that defines the boundary. To keep the uncoupled linear character of the algebraic system of Eqs. (7), the inner cycle (SLOR) iterations are always performed with Dirichlet boundary conditions. The system of equations obtained from the Neumann–Dirichlet boundary conditions is solved after each SLOR iteration at all the grid nodes where this type of boundary condition applies.

If, for example, we focus our attention in a ξ boundary, the grid coordinates derivatives in the ξ direction are obtained from the cubic "spline" representation of the boundary line. Using backward or forward second-order differences for the derivatives in the η direction, Eq. (1) becomes a nonlinear algebraic equation with ξ as the independent variable. The nonlinear equation is solved by Newton iteration and the cubic "spline" defines the coordinates (x, y) of the boundary node for the next SLOR iteration.

3.5. *Convergence Criteria*

The present method includes two iterative cycles: one refers to the determination of the distortion function, f; the other to the iterative solution of the linear system of algebraic equations included in each step of the determination of f. This second iterative cycle is referred to as the inner cycle and the iterative cycle of determination of f is referred to as the global cycle.

The convergence criterion used in the inner cycle is based on the maximum difference between grid coordinates in consecutive iterations,

$$\phi_i = \max(x_{i,j}^m - x_{i,j}^{m-1}, y_{i,j}^m - y_{i,j}^{m-1}), \tag{10}$$

where the superscript ^{m} refers to the inner cycle iteration.

For the iterative procedure of determination of f there are several alternatives to use as convergence criterion. One of the obvious choices is the parameter ϕ_f defined in Section 3.3 by Eq. (9). The grid orthogonality characteris-

tics may also be used like, for example, the maximum deviation from orthogonality, which is adopted by Allievi and Calisal in [12], or the maximum relative error in the Beltrami equations, (2), which is used by Duraiswami and Prosperetti in [13] to monitor the grid orthogonality characteristics. The maximum difference between grid coordinates of consecutive global iterations may also be used. In the present work we have analyzed the behaviour of six possible options:

1. The maximum relative difference of f between global iterations, ϕ_f.
2. The maximum deviation from orthogonality, MDO.
3. The maximum relative error of the Beltrami equations, MBE.
4. The maximum difference between grid coordinates in the first iteration of each inner cycle, ϕ_x.
5. The mean deviation from orthogonality, ADO.
6. The mean relative error of the Beltrami equations, ABE.

The maximum relative difference of f between global iterations, ϕ_f, is defined by Eq. (9).

The maximum and mean deviations from orthogonality, MDO and ADO are calculated from

$$\begin{aligned} \mathrm{MDO} &= \max(|90^\circ - \theta_{i,j}|), \\ \mathrm{ADO} &= \frac{1}{n_x - 2}\frac{1}{n_y - 2}\sum_{i=2}^{n_x}\sum_{j=2}^{n_y}(|90^\circ - \theta_{i,j}|), \end{aligned} \tag{11}$$

where

$$\theta = \arccos\left(\frac{g_{12}}{h_\eta h_\xi}\right). \tag{12}$$

The maximum and mean errors of the Beltrami equations, in percentages, MBE and ABE are calculated from

$$\mathrm{MBE} = 100 \max \left(\frac{\left| f_{i,j}\left(\frac{\partial x}{\partial \xi}\right)_{i,j} - \left(\frac{\partial y}{\partial \eta}\right)_{i,j}\right|}{\sqrt{J_{i,j}}}, \frac{\left| f_{i,j}\left(\frac{\partial y}{\partial \xi}\right)_{i,j} + \left(\frac{\partial x}{\partial \eta}\right)_{i,j}\right|}{\sqrt{J_{i,j}}} \right),$$

$$\mathrm{ABE} = \frac{50}{x_x - 2}\frac{1}{n_y - 2}\sum_{i=2}^{n_x}\sum_{j=2}^{n_y} \times \frac{\left| f_{i,j}\left(\frac{\partial x}{\partial \xi}\right)_{i,j} - \left(\frac{\partial y}{\partial \eta}\right)_{i,j}\right|}{\sqrt{J_{i,j}}} + \frac{\left| f_{i,j}\left(\frac{\partial y}{\partial \xi}\right)_{i,j} + \left(\frac{\partial x}{\partial \eta}\right)_{i,j}\right|}{\sqrt{J_{i,j}}} \tag{13}$$

where J is the Jacobian of the transformation given by

$$J = \sqrt{g} = \frac{\partial x}{\partial \xi}\frac{\partial y}{\partial \eta} - \frac{\partial x}{\partial \eta}\frac{\partial y}{\partial \xi}. \tag{14}$$

The first derivatives of the grid coordinates involved in the calculation of MDO, ADO, MBE, and ABE, are approximated by second-order central differences.

To avoid storing the initial approximation of each SLOR cycle, which represents the solution of the previous global iteration, the maximum difference between grid coordinates in consecutive global iterations is replaced by the maximum difference between grid coordinates of the initial iteration of the inner cycle,

$$\phi_x = \max(x^1_{i,j} - x^0_{i,j}, y^1_{i,j} - y^0_{i,j}), \tag{15}$$

where the superscripts refer to iterations of the inner cycle.

4. CONVERGENCE STUDIES

Two geometries were selected to examine the convergence characteristics of the method. The first geometry has been widely used as a test case of orthogonal grid generators since the work of Haussling and Coleman in 1981 [2]. It is a concave region limited by the lines $x = 0$, $x = 1$, $y = 0$, and $y = 0.75 + 0.25\sin(\pi(0.5 + 2x))$. The second test case was used by Visbal and Knight in [3], and it is a rather demanding test case for particular choices of the boundary point distribution. It is a region limited by two nonconcentric half-circles and the x axis, $y = 0$. The smallest half-circle has a diameter of 1 and the largest one has a diameter of 3. In both geometries, the grid coordinates are of order 1, which can always be achieved by making x and y dimensionless using the reference length scale.

The influence of the convergence criterion of the inner cycle, SLOR solution, on the global cycle was investigated in previous test runs. The results obtained showed that the global iteration convergence history is independent of the inner cycle criterion if it is assumed that the inner cycle is stopped when $\phi_i \le 1.0 \times 10^{-6}$. This convergence criterion has been adopted in all the applications here presented. The calculations were performed using double precision in a 32-byte precision machine.

Four test cases with Dirichlet boundary conditions in all the boundaries have been selected. These test cases will be denoted in the following way:

1. Case A (Concave region). The difference of the y coordinate, Δy, of the grid nodes along the boundaries $x = 0$ and $x = 1$ is constant. Δx is constant for the other two boundaries.
2. Case B (Concave region). This test case is similar to Case A. A different grid node distribution is specified in the boundary at $x = 1$.

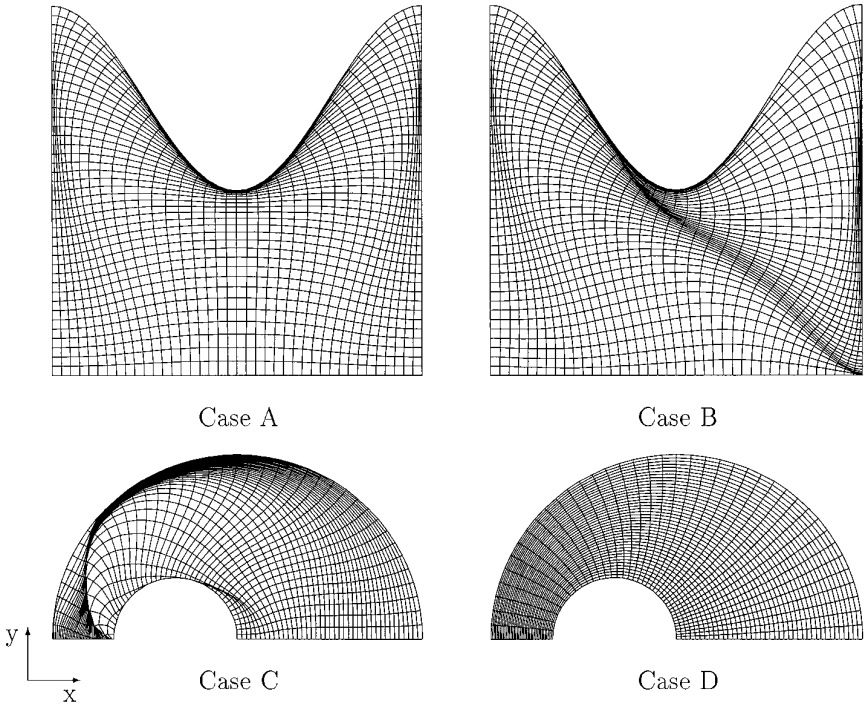

FIG. 2. Test cases for the convergence criteria of the method. Grids obtained after 400 iterations, with specified boundary point distribution in all the boundaries.

3. Case C (Region limited by two half-circles and the x axis). The grid nodes along the four boundaries are specified with a constant distance between grid nodes of each boundary.

4. Case D (Region limited by two half-circles and the x axis). This test case is similar to case C. A different grid node distribution is specified along the half-circle of smallest diameter.

The grids obtained after 400 iterations of the global iteration cycle are illustrated in Fig. 2. The grids of the four test cases have 41×41 grid nodes. The values of ϕ_x, ϕ_f, MDO, MBE, ADO, and ABE of the last iteration are summarized in Table I.

Test Cases A and B show that it is possible to obtain orthogonal grids in this concave region specifying different boundary point distributions. The grid obtained for Test Case C has regions where one of the scale factors, h_ξ or h_η, tends to zero. With the specified boundary point distribution of this test case, the orthogonality condition originates regions where several grid lines tend to collapse into one, forming a sort of ''surface of discontinuity'' in the domain. The highly distorted regions of the grid close to these ''fronts'' exhibit large deviations from orthogonality, causing the large values obtained for MDO and MBE. Nevertheless, the mean values, ADO and ABE, indicate that these large deviations from orthogonality occur only locally. With the boundary distribution used in Test Case D a perfectly smooth grid is obtained.

The difficulties in the determination of the distortion function in Test Case C were found for several initial conditions and for different values of the inner cycle convergence criterion, ϕ_i. The grid of Test Case C was also calculated, imposing that the scale factors h_ξ and h_η must be greater than or equal to 1.0×10^{-6}. The grid line pattern obtained after 400 iterations of the global iteration cycle is almost identical to the one plotted in Fig. 2. The restriction im-

TABLE I

Values of Maximum Deviation from Orthogonality, MDO, Maximum Beltrami Error, MBE, Mean Deviation from Orthogonality, ADO, Mean Beltrami Error, ABE, Maximum Relative Difference in the Distortion Function, ϕ_f, and Maximum Difference between Grid Coordinates in the First Iteration of the Inner Cycle, ϕ_x, at the 400th Iteration of the Global Cycle

Test case	MDO	MBE	ADO	ABE	$\log_{10}(\phi_f)$	$\log_{10}(\phi_x)$
A	0.87	2.90	0.12	0.12	−2.46	−4.54
B	2.28	7.33	0.25	0.25	−2.37	−4.13
C	71.2	23.4	1.44	0.65	−0.41	−3.49
D	0.20	0.18	0.04	0.03	−4.13	−5.24

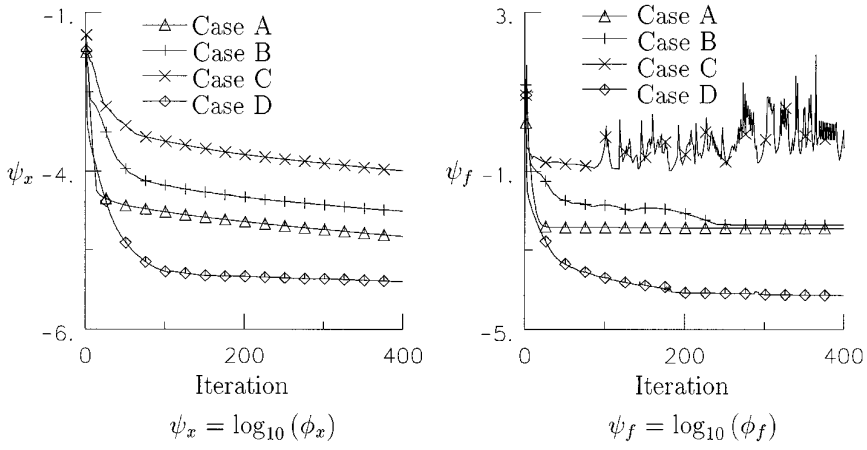

FIG. 3. Convergence history of the distortion function and grid coordinates in the Test Cases A, B, C, and D.

posed on the scale factors has no effect in the values of MBE and ABE, but MDO is reduced to 17° and ADO to 1.0°. These results suggest that the orthogonality condition and the specified boundary point distribution are responsible for the ''surface discontinuities'' obtained in Test Case C. The perfectly smooth grid obtained in Test Case D, with the same boundary geometry, shows that the specification of the boundary point distribution in all the boundaries may be troublesome in orthogonal grid generation, even for simple geometries.

The history of ϕ_x, ϕ_f, along the 400 iterations is depicted in Fig. 3. The evolutions of ϕ_x in the four test cases have a similar pattern. A large decay is obtained in the initial iterations, followed by a much smaller decay which seems to remain constant thereafter. The order of magnitude of ϕ_x, where the decay of ϕ_x is reduced, is different in the four test cases. The difference between Test Cases C and D, which correspond to the same geometry, is almost two orders of magnitude. The evolutions of ϕ_f have the same initial region of large decay, which is followed by an almost constant value, with the exception of Test Case C. In this test case, the regions where the scale factors tend to zero cause several oscillations in the f determination, which becomes unstable. However, these oscillations seem to occur around a constant value of ϕ_f. These results suggest that the f determination has a maximum level of precision which can be obtained.

The evolution of the four parameters that characterize the grid orthogonality, MDO, MBE, ADO, and ABE along the global cycle iterations are plotted in Fig. 4. The deviation from orthogonality and the Beltrami error give similar information. The mean values, ADO and ABE, show a strong reduction in the initial iterations followed by an almost constant value, with the exception of Test Case C, where the instabilities caused by the ''shocks'' are reflected in ADO. The maximum differences, which do not include Test Case C, show a strong reduction in the initial iterations, followed by a small increase which seems to be negligible only in Test Case D. The iteration where the minimum values of MDO and MBE occur is closely related to the iteration where ϕ_f becomes almost constant.

To clarify the reason why ϕ_f has a lower limit, Test Case A was repeated using single precision. The constant value of ϕ_f after a few iterations remains unchanged, which excludes roundoff error as the origin of this lower limit of

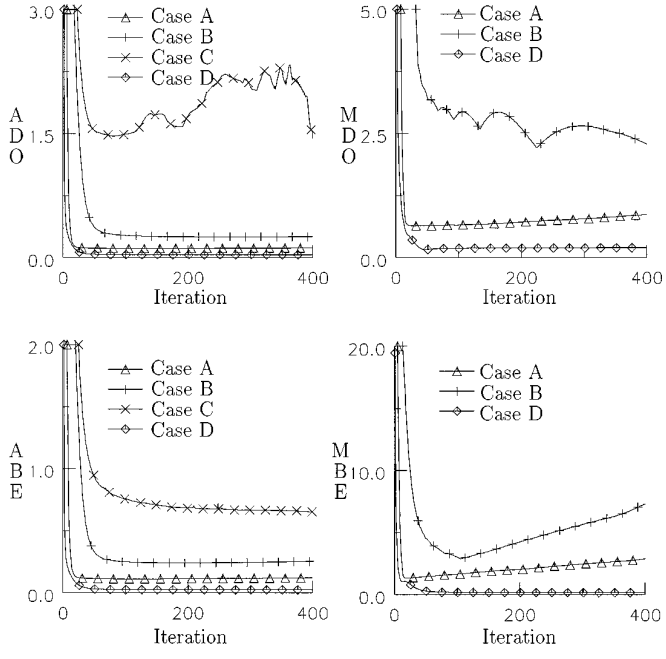

FIG. 4. Evolution of the maximum deviation from orthogonality, MDO, mean deviation from orthogonality, ADO, maximum Beltrami error, MBE, and mean Beltrami error, ABE, in the Test Cases A, B, C, and D.

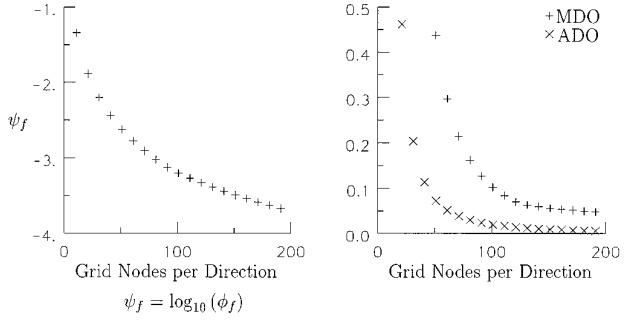

FIG. 5. Maximum relative difference of the distortion function between global iterations, ϕ_f, and maximum and mean deviations from orthogonality, MDO and ADO, as a function of the number of grid nodes per direction. Test Case A with 200 global iterations.

ϕ_f. The truncation error of the numerical solution of the system of partial differential equations is related to the number of grid nodes used per direction. To evaluate its influence on the behaviour of ϕ_f, Test Case A was repeated using different numbers of grid nodes, ranging from 11 to 191 nodes per direction. Figure 5 illustrates the values of ϕ_f after 200 iterations of the global cycle as a function of the number of grid nodes per direction. The values of MDO and ADO are also depicted in Fig. 5. The results obtained show that the lower limit of ϕ_f is related to the truncation error of the finite-difference approximations used in the discretization of the system of partial differential equations. The reduction of the truncation error reduces also the deviation from orthogonality in the grid. A similar conclusion is obtained if this test is repeated for Test Cases B or D. In Test Case C the solution is conditioned by the ''shocks'' and so a similar test is not conclusive.

These convergence studies suggest that none of the six parameters investigated should be used alone as the convergence criterion of the global iteration process. The present option is to use ϕ_x and ϕ_f to define the convergence criteria of the global iteration. The calculation is assumed to be converged if ϕ_x becomes smaller than a specified tolerance. In addition, if the difference of ϕ_f between two consecutive iterations becomes smaller than a specified value the global iteration is assumed to be converged and the grid is the solution of the inner cycle with the converged distortion function.

4.1. *Boundary Conditions*

The use of different types of boundary conditions is investigated with four test cases, where 400 global iterations were performed in 41 × 41 grids. These four test cases will be denoted in the following way:

1. Case E (Concave region). This test case corresponds to Case B. The boundary point distribution is specified in all the boundaries and the distance of the first grid node to the boundary is specified along the boundary $y = 0$.

2. Case F (Region limited by two half-circles and the x axis). This test case corresponds to Case D. The grid node distribution and the distance of the first grid node to the boundary is specified in all the boundaries.

3. Case G (Region limited by two half-circles and the x axis). This test case corresponds to Case C. Neumann–Dirichlet boundary conditions are applied at the half-circle of largest diameter.

4. Case H (Region limited by two half-circles and the x axis). This test case is equivalent to Case G, but in addition the distance of the first grid node to the boundary is specified at the half-circle of largest diameter.

The grids generated for Test Cases E and F are plotted in Fig. 6. The global iteration cycle diverges for Test Cases G and H, where Neumann–Dirichlet boundary conditions are applied at the half-circle of largest diameter. The convergence histories of the distortion function and of the grid coordinates are plotted in Fig. 7. Test Cases G and H, where the distance of the first grid node to the boundary is specified, have a convergence history similar to the one obtained for Test Cases B and D, where only the boundary point distribution is specified. The divergence of the global iteration cycle is clear in Cases G and H.

The evolutions of the four parameters that characterize the grid orthogonality, MDO, MDE, ADO, and ABE are depicted in Fig. 8. The values of ϕ_x, ϕ_f, MDO, MBE, ADO, and ABE of the last iteration are summarized in Table II. The results of Test Cases G and H show the divergence of the global iteration cycle, following a few initial iterations where a big improvement of the orthogonality characteristics is obtained. The pattern of the evolutions of Test Cases E and F is similar to the one obtained with only the boundary point distribution specified. However, the precision of the f determination is smaller than the one obtained in Test Cases B and D, which makes the values of MDO and MBE in Test Cases E and F larger than the ones obtained in Test Cases B and D.

These test cases show that it is possible to generate orthogonal grids with the distance of the first grid node to the boundary specified, using the present generating system. The behaviour of the iterative solution with the Neumann–Dirichlet boundary conditions suggests that the Dirichlet boundary conditions should be used in all the boundaries when the distortion function is calculated from its definition equation in all the domain.

5. APPLICATIONS

The present generating system was applied to several geometries. The selected geometries have been used by different authors for test cases of orthogonal grid genera-

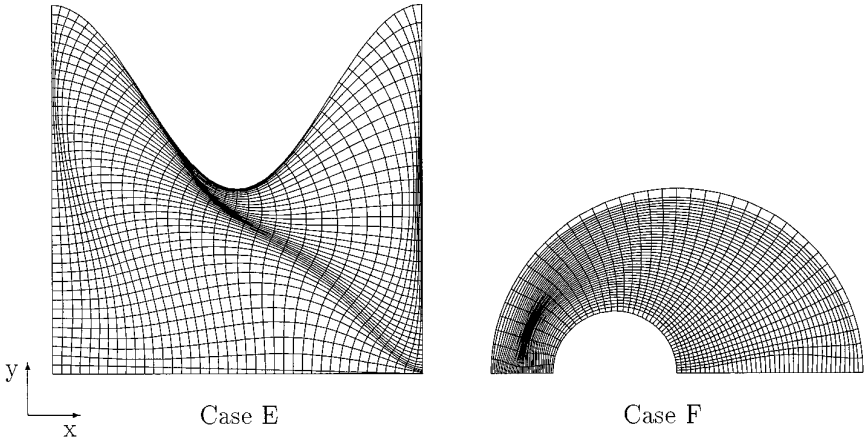

FIG. 6. Test cases for the convergence criteria of the method. Grids obtained after 400 iterations, with specified distance of the first grid node to the boundary and specified boundary point distribution.

tors, or, in some cases, have a relevant role in computational fluid dynamics. The calculations were performed with a convergence criterion of $\phi_i \leq 1.0 \times 10^{-6}$ for the SLOR solution of the inner cycle. The convergence criterion of the global cycle is $\phi_x \leq 1.0 \times 10^{-5}$. The distortion function is considered to be converged when the difference of ϕ_f between consecutive iterations becomes smaller than 1.0×10^{-4} in two consecutive iterations. The different applications will be denoted by the number of the figure where the grids are plotted. The values of ϕ_f, MDO, MBE, ADO, and ABE of all the applications are summarized in Table III.

The orthogonality characteristics of the grids of the six test cases used in the convergence studies, calculated with the present convergence criterion, are also included in Table III. The comparison of the present values with the values obtained after 400 global cycle iterations shows that a number of global iterations much smaller than the one used in the convergence studies is sufficient to obtain the grid, without a significant decrease in its orthogonality. In some of the test cases, the value of MDO is even reduced. In Test Case 2C, the value of MDO is significantly reduced because the convergence criterion used in the f determination freezes the distortion function after a few iterations, reducing the intensity of the "shocks."

The first geometry has been used by several authors [1, 5, 6, 12, 13]. It is a domain limited by the coordinate axes and the lines $y = 1$ and $x = \frac{1}{2} + \frac{1}{6}\cos(\pi y)$. Figure 9 presents three grids of 41×41 nodes generated in this domain. Grids 9a and 9b have two different boundary point distri-

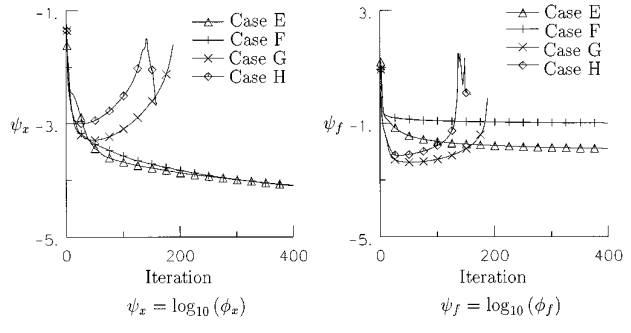

FIG. 7. Convergence history of the distortion function and grid coordinates in the Test Cases A, B, C, and D.

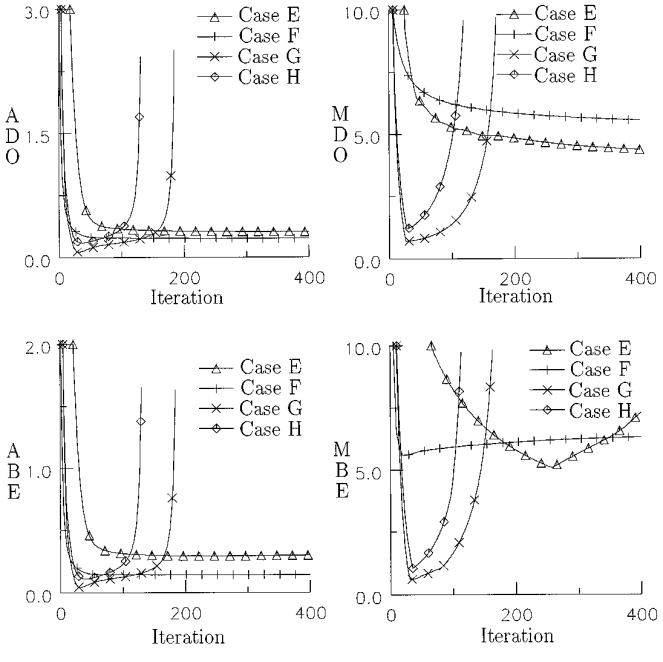

FIG. 8. Evolution of the maximum deviation from orthogonality, MDO, mean deviation from orthogonality, ADO, maximum Beltrami error, MBE, and mean Beltrami error, ABE, in the Test Cases A, B, C, and D.

TABLE II

Values of Maximum Deviation from Orthogonality, MDO, Maximum Beltrami Error, MBE, Mean Deviation from Orthogonality, ADO, Mean Beltrami Error, ABE, Maximum Relative Difference in the Distortion Function, ϕ_f, and Maximum Difference between Grid Coordinates in the First Iteration of the Inner Cycle, ϕ_x, at the 400th Iteration of the Global Cycle

Test case	MDO	MBE	ADO	ABE	$\log_{10}(\phi_f)$	$\log_{10}(\phi_x)$
E	4.36	7.32	0.31	0.30	−1.90	−4.09
F	5.54	6.31	0.23	0.14	−1.00	−4.10

butions. Grid 9c has the boundary point distribution of grid 9b and, in addition, the distance of the first grid node to the boundary is specified in all the boundaries. The maximum deviations from orthogonality of grids 9a, 9b, and 9c are, respectively, 0.20°, 1.45°, and 5.67°. The values of MDO seem to be related to the distortions imposed by the boundary conditions, which are reflected in the precision of the distortion function calculations. The orthogonality characteristics of grid 9a, which has a regular boundary point distribution, are similar to the ones presented by Duraiswami and Prosperetti in [13]. We note that the method presented in [13] uses Neumann–Dirichlet boundary conditions in the four boundaries, which means that it does not have direct control on the boundary point distribution. The method of Allievi and Calisal [12] with complete boundary point correspondence, produces grids with larger deviations from orthogonality than the present method. However, in [12], the number of grid nodes used, 16×16, is smaller than the one used in the present grids.

The second application is included in the paper of Duraiswami and Prosperetti in [13]. It is a unit square with a half-circle on each side. A 41×41 grid in this domain is illustrated in Fig. 10. In this example, the grid nodes are equidistant along the boundaries. The value of MDO, 12.5° is the largest one obtained, with the exception of Test Case 2C. The maximum deviation from orthogonality occurs in the vicinity of the corners of the domain, where the angle between the grid lines is 270°. This poor performance of the method is due to a local effect, as shown by the mean values of the deviation from orthogonality and Beltrami error. The present method is not able to deal satisfactorily with internal angles which are larger than 180°. In this case, the present handling of the grid coordinates at the corners of the control "volume" does not ensure that the interpolated coordinates are within the domain. If the distance of the grid nodes to the corners of the domain is reduced in grid 10, the method produces a grid which has a negative

TABLE III

Values of Maximum Deviation from Orthogonality, MDO, Maximum Beltrami Error, MBE, Mean Deviation from Orthogonality, ADO, Mean Beltrami Error, ABE, Maximum Relative Difference in the Distortion Function, ϕ_f, for the Converged Solutions of All the Test Cases

Test case	Number of grid nodes	MDO	MBE	ADO	ABE	$\log_{10}(\phi_f)$	Global iterations
2A	41×41	0.64	1.36	0.12	0.12	−2.40	27
2B	41×41	3.18	4.06	0.31	0.28	−1.81	64
2C	41×41	44.2	65.6	2.01	1.43	−0.77	32
2D	41×41	0.25	0.57	0.05	0.04	−3.02	34
6E	41×41	5.16	7.34	0.34	0.30	−1.67	126
6F	41×41	5.91	6.07	0.23	0.14	−0.94	173
9a	41×41	0.20	0.49	0.04	0.06	−2.93	21
9b	41×41	1.45	4.78	0.24	0.40	−2.04	66
9c	41×41	5.67	11.4	0.34	0.54	−1.54	106
10	41×41	12.5	22.0	0.18	0.20	−1.75	66
11	41×41	0.42	0.50	0.07	0.04	−2.48	21
12a	41×41	0.10	0.11	0.02	0.02	−2.98	23
12b	41×41	1.05	2.93	0.19	0.21	−2.00	24
13a	41×41	1.03	1.06	0.42	0.24	−1.95	46
13b	41×41	1.37	1.60	0.47	0.18	−1.89	45
14a	41×41	1.93	1.93	0.11	0.06	−1.99	22
14b	41×41	4.41	2.26	0.18	0.07	−1.53	41
15a	29×55	2.93	3.36	0.37	0.20	−2.17	100
15b	29×55	3.78	3.27	0.62	0.24	−1.45	30
16a	29×55	3.83	1.44	0.29	0.15	−2.38	59
16b	29×55	5.37	7.03	0.41	0.22	−1.60	48

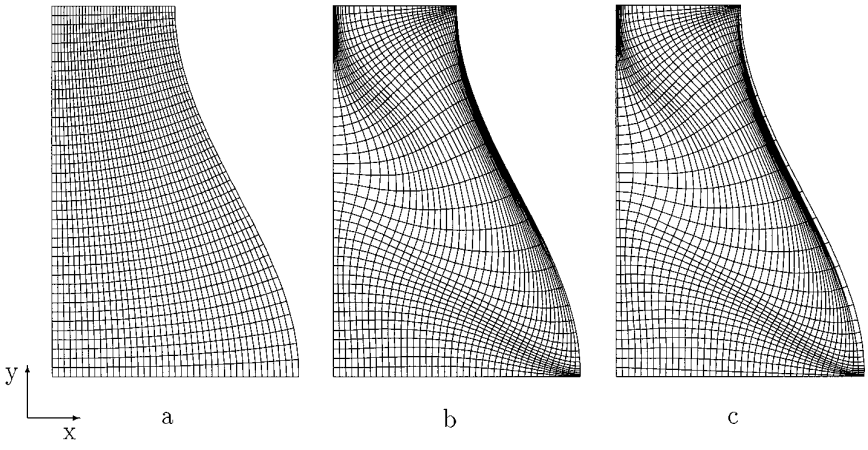

FIG. 9. Grids on a domain limited by the coordinate axes and the lines $y = 1$ and $x = \frac{1}{2} + \frac{1}{6}\cos(\pi y)$. Distance of the first grid node to the boundary specified in grid *c*.

Jacobian close to the corner of the domain. This type of geometry with internal angles larger than 180°, requires modifications of the present discretization scheme.

The third geometry is also used by Duraiswami and Prosperetti in [13]. It is a lune with the two sides given by the lines $y = x(1 - x)$ and $y = -x(1 - x^2)$. In this example, two of the computational domain boundaries collapse into a single node in the physical domain, which means that the Jacobian of the transformation is zero at these boundaries. A 41×41 grid generated in this domain is illustrated in Fig. 11. The orthogonality characteristics, MDO and MBE, of the grid are very satisfactory and the number of global iterations required is the lowest of all the examples. For this geometry, the grid orthogonality characteristics are similar to the ones presented by Duraiswami and Prosperetti in [13].

The next example is also a degenerate quadrilateral [13]. It is a trilateral region limited by the lines $y = x$, $y = -x$ and the line defined by $x = r \cos \theta$, $y = r \sin \theta$ with $r(\theta) = 1 - 0.1 * (1 - \sin \theta)$. In this example, two 41×41 grids are presented. The distance of the first grid node to the curved boundary has been specified in grid 12b. The values of MBO and MBE are small and the number of global iterations required is also small. The orthogonality characteristics of the present grids are again comparable to the grids presented in [13].

The applications presented in Figs. 13 and 14 are 41×41 C-grids and O-grids around a NACA 0015 airfoil. The examples include grid line distributions in the normal direction with highly stretched regions close to the airfoil surface, which are typical of viscous flow calculations. For grids 13b and 14b the distance of the first grid node to the airfoil surface is specified. In the O-grid, the method is able to handle properly the trailing edge region, where the angle between grid lines is almost 180°, keeping small the deviations from orthogonality in the domain.

Figures 15 and 16 include 29×55 grids of two typical

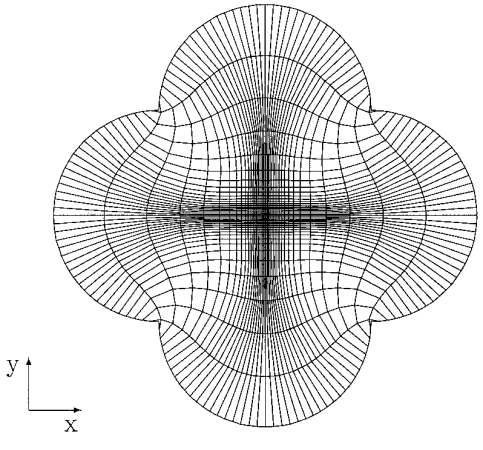

FIG. 10. Grid on a domain constructed with four half-circles at the sides of a unit square.

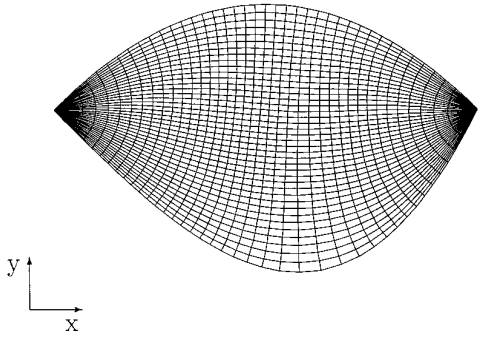

FIG. 11. Grid on a domain limited by the lines $y = x(1 - x)$ and $y = -x(1 - x^2)$.

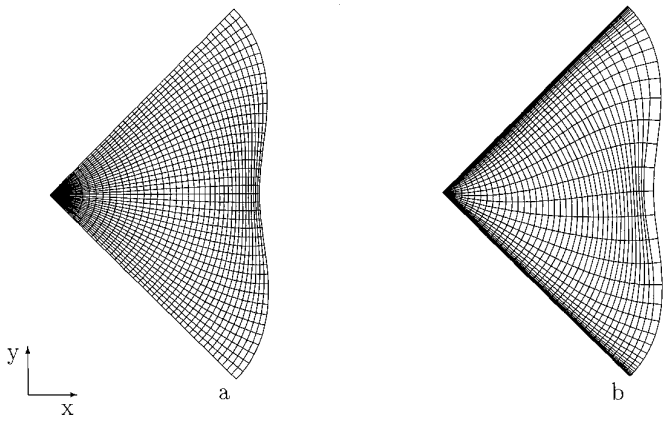

FIG. 12. Grids on a trilateral with sides $y = x$, $y = -x$ and $x = r \cos \theta$, $y = \sin \theta$, where $r(\theta) = 1 - 0.1 * (1 - \sin \theta)$. Distance of the first grid node to the boundary specified in grid b.

cross sections of a ship stern flow calculation. The geometry of Fig. 15, which corresponds to a typical cross section of a tanker, has the difficulties imposed by the change in curvature of the ship surface. The grid 15b was generated with a specified distance of the first grid node to the boundary at the ship surface and at the opposite boundary. The grid line stretching imposed at the boundary is reflected in the interior grid lines. In grid 15b, the distance of the first grid node to the ship surface is actually constant. The examples of Fig. 16 correspond to a typical wake cross section. In this case, the grid includes a singularity at one of the corners of the computational domain, where the angle between the grid lines is 180°. The grid 16b was generated with a specified distance of the first grid node to the boundary at the ship surface and at the opposite boundary. The method is able to deal with this type of singularities and with grid line stretching, producing grids with reduced deviations from orthogonality.

In the examples presented in Figs. 13b, 14b, 15b, and 16b, the maximum difference between the specified grid spacing at the boundaries and the grid spacing of the generated grids is less than 3.5% of the specified distance. These results show that the method is able to respect the specified grid spacing at the boundaries without losing grid orthogonality.

The maximum deviations from orthogonality and maximum Beltrami errors obtained in all the examples show that the values of MDO and MBE are strongly dependent on the precision with which the distortion function is calculated.

6. CONCLUSIONS

A method for the generation of 2D orthogonal grids with control of the boundary point distribution has been numerically investigated. The method is based on a system of partial differential equations and on an iterative determination of the distortion function from its definition equation. The boundary point distribution is specified in all the boundaries, and, in addition, the distance of the first grid node to the boundary may also be specified.

The convergence studies performed showed that the maximum deviation from orthogonality of the generated grids is related to the truncation error of the finite-difference approximations used in the discretization. These studies also indicate that Neumann–Dirichlet boundary conditions cannot be used when the distortion function is calculated iteratively from its definition equation.

In some geometries and for certain boundary point distributions the orthogonality constraint in the domain may originate the collapse of several grid lines into one, causing

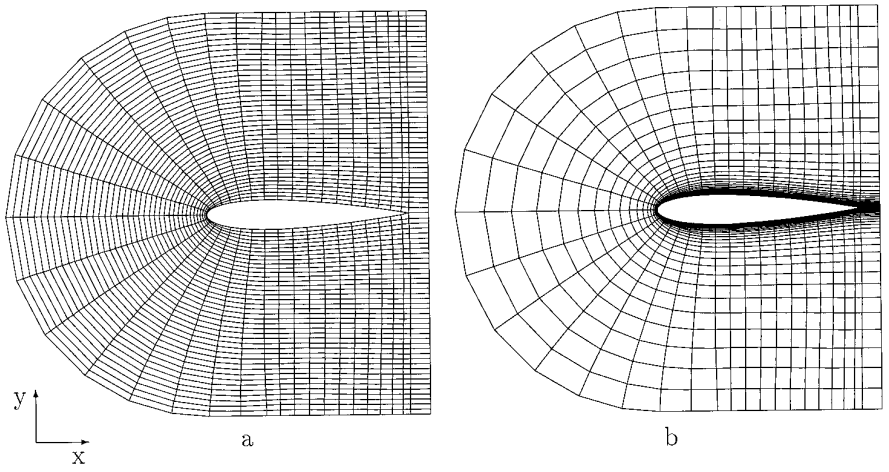

FIG. 13. C-grids around a NACA 0015 airfoil. Distance of the first grid node to the airfoil surface specified in grid b.

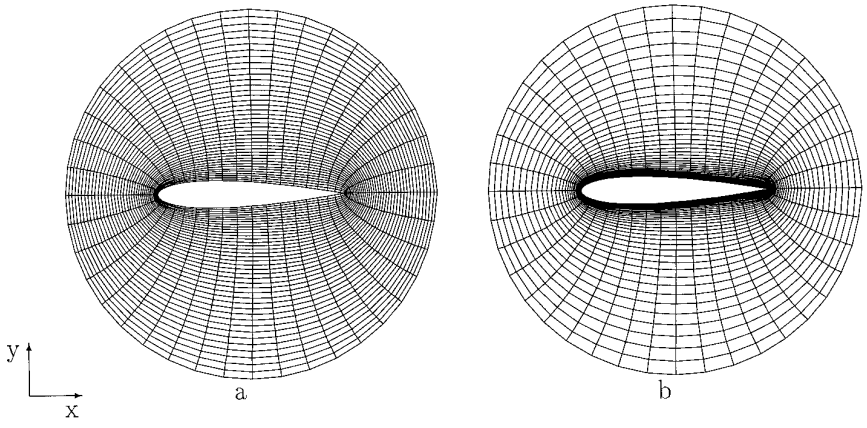

FIG. 14. O-grids around a NACA 0015 airfoil. Distance of the first grid node to the airfoil surface specified in grid b.

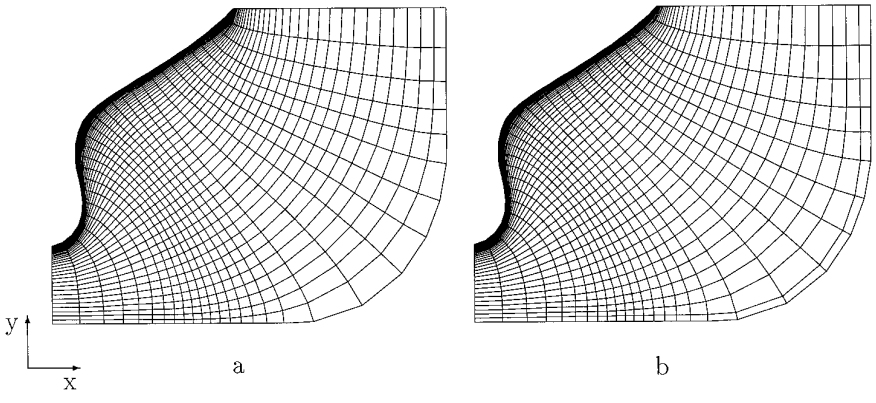

FIG. 15. Grids around a typical cross section of a ship stern. Distance of the first grid node to the boundary specified in grid b.

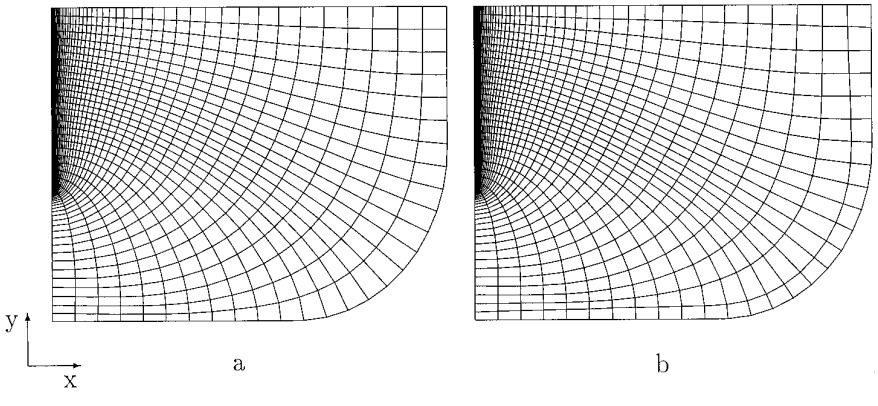

FIG. 16. Grids on a typical wake cross section of a ship stern flow calculation. Distance of the first grid node to the boundary specified in grid b.

convergence difficulties. Locally, these regions where one of the scale factors tends to zero have large deviations from orthogonality.

The method is not able to deal with domains including internal angles larger than 180°. The present discretization technique does not guarantee that the coordinates of the corners of the control ''volume'' remain inside the domain. However, it handles satisfactorily domains, including grid singularities at the sides or corners of the computational domain, if the interior angles remain below 180°.

The application of the method to several difficult geometries, including degenerate quadrilaterals and grid singularities, showed that it is possible to generate orthogonal grids with direct control of the boundary point distribution. Furthermore, the present examples show that it is also possible to specify the distance of the first grid node to the boundary, which may represent a very attractive feature for some applications like, for example, viscous flows in computational fluid dynamics.

The application of the method to grids around airfoils and typical cross sections of ship sterns, using highly stretched grid line distributions, typical of viscous flow calculations, showed that the present method is a powerful tool for orthogonal grid generation.

REFERENCES

1. C. D. Mobley and R. J. Stewart, *J. Comput. Phys.* **34,** 124 (1980).
2. H. J. Haussling and R. M. Coleman, *J. Comput. Phys.* **43,** 373 (1981).
3. L. Visbal and D. Knight, *AIAA J.* **20,** 305 (1982).
4. G. Ryskin and L. G. Leal, *J. Comput. Phys.* **50,** 71 (1983).
5. E. D. Chikhliwala and Y. C. Yortsos, *J. Comput. Phys.* **57,** 391 (1985).
6. R. Arina, ''Orthogonal Grids with Adaptive Control,'' in *1st International Conference on Numerical Grid Generation in CFD*, edited by J. Hauser and C. Taylor (Pineridge Press, Swansea, 1986).
7. E. P. Ascoli, D. S. Dandy, and L. G. Leal, *J. Comput. Phys.* **72,** 513 (1987).
8. M. R. Albert, ''Orthogonal Curvilinear Coordinate Generation for Internal Flows, in Numerical Grid Generation in Computational Fluid Mechanics'' (Pineridge Press, Swansea, 1988).
9. P. Daripa, *J. Comput. Phys.* **96,** 229 (1991).
10. S. Saha and B. C. Basu, *AIAA J.* **29,** 1340 (1991).
11. G. Moretti, *AIAA J.* **30,** 933 (1992).
12. A. Allievi and S. M. Calisal, *J. Comput. Phys.* **98,** 163 (1992).
13. R. Duraiswami and A. Prosperetti, *J. Comput. Phys.* **98,** 254 (1992).
14. J. F. Thompson, F. C. Thames, and C. W. Mastin, *J. Comput. Phys.* **24,** 274 (1977).
15. J. L. Steger and R. L. Sorenson, *J. Comput. Phys.* **33,** 405 (1979).
16. J. F. Thompson and Z. U. A. Warsi, *J. Comput. Phys.* **47,** 1 (1982).
17. O. Lehto and L. I. Virtanen, *Quasi-Conformal Mappings in the Plane* (Springer-Verlag, Berlin, 1973).
18. L. W. Ehrlich, *J. Comput. Phys.* **44,** 31 (1981).
19. J. F. Thompson, *AIAA J.* **22,** 1505 (1984).